JOURNAL OF GUIDANCE, CONTROL, AND DYNAMICS
Vol. 33, No. 2, March–April 2010

Algorithm for Conformance Monitoring in Air Traffic Control

Chze Eng Seah,* Alinda Aligawesa,† and Inseok Hwang‡
Purdue University, West Lafayette, Indiana 47907

DOI: 10.2514/1.44839

Conformance monitoring in air traffic control is an approach that is used to detect any deviations of the aircraft from its cleared (or planned) flight path that might compromise safety and efficiency. This task is made difficult by the fact that some deviations are normally expected of a conforming aircraft due to uncertainties. In this paper, a conformance monitoring algorithm that uses a stochastic linear hybrid system model is proposed. The stochastic linear hybrid system model divides the aircraft dynamics into a number of flight modes and is able to describe the random deviations in (conforming) aircraft trajectories. The detection of any nonconforming trajectories is determined by a fault detection technique. First, a hybrid estimation algorithm is used to estimate the hybrid state of the stochastic linear hybrid system and generate a residual vector based on the measurements. The statistical characteristics of the residual expected of a conforming aircraft are derived. Then, a statistical decision test is used to detect any deviation of the observed residual from the expected residual. Two illustrative examples are presented to demonstrate the performance of the proposed algorithm.

I. Introduction

CONFORMANCE monitoring in air traffic control (ATC) is an approach that is used to monitor and detect any deviations of an aircraft flight path from the assigned flight plan that might compromise safety or efficiency [1]. The Federal Aviation Agency has projected that, by the year 2025, the number of aircraft passengers may increase two to three times [2]. A new concept of operation, known as the Next Generation Air Transportation System (NEXTGEN), has been proposed to meet these challenges [3]. The proposed concept of operation has identified major changes in areas, such as air traffic management, air traffic surveillance, and system infrastructure. Under the NEXTGEN, a larger number of aircraft are expected to operate with reduced separation thresholds between aircraft within a given airspace. The new concept of operation also allows aircraft the flexibility of changing flight routes (or flight plans) in response to changing conditions [4,5]. Furthermore, the responsibility of ensuring safe separation may be delegated to individual aircraft. With these changes, it would be important to have a conformance monitoring tool for monitoring the aircraft movements. Currently, the task of conformance monitoring is performed by air traffic controllers by comparing the estimated aircraft position, heading, speed, etc. (computed with observed aircraft positions from radar surveillance) with those expected based on clearances or flight plans. If the differences between the observed and expected positions exceed some allowable deviations, nonconformance can be determined [1]. Because of many other tasks required of an air traffic controller, this method does not necessarily give the performance that may be required in the future with higher traffic levels, and hence a decision support algorithm may be beneficial. The conformance monitoring task will be even more difficult in future ATC operations. Apart from the more complex operating scenarios, different aircraft will have very different navigation capabilities, due to the different levels of equipment onboard. Therefore, there is a need to investigate conformance monitoring tools that are capable of addressing both complex air traffic operations and various levels of navigation uncertainties.

There are some recent research interests on conformance monitoring, due to the increased demand for higher capacity in the National Airspace System [1,6,7]. Brinton and Atkins have analyzed the performance of a prototype algorithm on taxi conformance monitoring, with an emphasis on the possibility of improving the existing conformance monitoring algorithms to increase safety and reduce the controllers' workloads [7]. Reynolds and Hansman have proposed a conformance monitoring scheme, based on fault detection techniques, by testing the conformance residuals (CRs) generated (based on the difference between the observed and expected state values of an aircraft [1,6]). Their work focuses on investigating issues that arise in applying the conformance monitoring scheme to different operational scenarios. They have identified and illustrated several challenges in aircraft conformance monitoring due to uncertainties in aircraft trajectory deviations. For example, the CRs of a conforming aircraft could be very large due to uncertainty at a waypoint transition, and this results in a higher false alarm rate (FAR), given the mean detection delay. Thus, there is still much work to be done to improve the performance of existing conformance algorithms, such as to achieve a rapid detection of nonconformance during waypoint transitions.

In this paper, motivated by the work of Reynolds and Hansman [1], a conformance monitoring algorithm, based similarly on a fault detection concept, is proposed. The general idea of the conformance monitoring scheme is illustrated in Fig. 1. Here, the actual system represents the dynamics of an aircraft, and the measurements are its observed trajectory. The model of the system describes the expected behavior of a conforming aircraft. In practice, for ATC applications, the command input is not known exactly, but it can be inferred from flight plan and clearance information. The conformance monitoring algorithm is implemented as a fault detection function, which consists of a residual generation scheme and a decision making scheme. The residual generation scheme generates a vector known as the residual, which is used to test for conformance or nonconformance by the decision making scheme. The contributions of this paper are: 1) the development of an effective residual generation scheme that generates a residual with zero mean when the observed aircraft trajectory conforms to our aircraft dynamics model; 2) the derivation of approximate statistical characteristics of the residual, which

Presented as Paper 6170 at the AIAA Guidance, Navigation, and Control Conference, Chicago, IL, 10–13 August 2009; received 9 April 2009; revision received 23 October 2009; accepted for publication 25 October 2009.

*Graduate Student, School of Aeronautics and Astronautics; seah@purdue.edu.

†Graduate Student, School of Aeronautics and Astronautics; aaligawe@purdue.edu.

‡Assistant Professor, School of Aeronautics and Astronautics; ihwang@purdue.edu. Member AIAA.

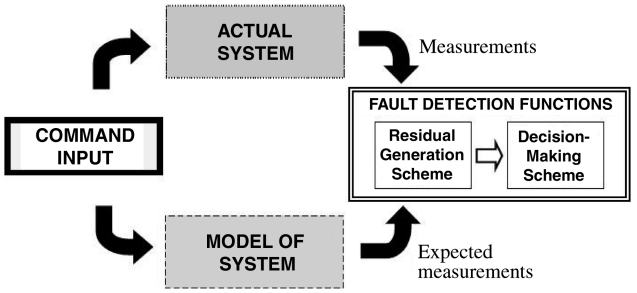

Fig. 1 Model-based fault detection concept.

facilitates the implementation of the statistical decision making algorithm; and 3) the use of a model that can accurately represent the aircraft dynamics, as well as its navigation errors, flight plans, and air route structures. In most other conformance monitoring algorithms, such as that in Reynolds and Hansman [1], the aircraft model assumes that aircraft follow the planned flight paths without any navigation errors. To account for navigation uncertainties, these algorithms use higher detection thresholds during decision making, and this will result in higher detection delays. Our aircraft model includes a description of aircraft navigation uncertainties about flight plans or standard air routes. These uncertainties may be determined based on the required navigation performance (RNP) for current ATC operations, or based on the aircraft navigation capabilities in the NEXTGEN. As a result, our conformance monitoring algorithm uses smaller detection thresholds and yields smaller detection delays, compared with algorithms that do not account for the aircraft navigation uncertainties directly. The proposed algorithm could be applied to current ATC scenarios with radar surveillance systems, as well as future ATC scenarios, with measurements reported by automatic dependent surveillance-broadcast (ADS-B) systems.

This paper is organized as follows. Section II presents the aircraft model, which is used to describe the trajectory of a conforming aircraft. The aircraft model is a hybrid system that consists of both the continuous state (e.g., aircraft positions) and the discrete state (or flight modes). Section III presents the conformance monitoring algorithm, which consists of the residual generation scheme and the decision making scheme. Approximate statistical characteristics of the residual are derived to facilitate decision making. In Sec. IV, two simulation examples are presented to illustrate the performance of the proposed algorithm and compared with other conformance monitoring algorithms. The scenario in the first example involves a waypoint transition in a horizontal plane, and the other involves an altitude transition in the vertical plane. These scenarios illustrate the challenges in conformance monitoring due to uncertainties in aircraft operations. The simulation results validate that the proposed algorithm yields small detection delays with low given FARs in such challenging scenarios. Conclusions are given in Sec. V.

II. Aircraft Model

The dynamics of the aircraft are modeled as a stochastic linear hybrid system (SLHS), which consists of both the continuous state and the discrete state. The continuous state describes the aircraft position, velocity, etc., and the discrete state describes the aircraft flight modes, such as constant velocity (CV), coordinated turn (CT), etc. The continuous state dynamics and measurements of the SLHS model are given by

$$x(k) = A_{q(k)}x(k-1) + w_{q(k)}(k) \tag{1}$$

$$z(k) = C_{q(k)}x(k) + v_{q(k)}(k) \tag{2}$$

where $x(k) \in \mathbb{R}^n$ is the continuous state; $z(k) \in \mathbb{R}^p$ is the measurement vector; $q(k) \in \{1, 2, \ldots, n_d\}$ is the discrete state or flight mode at a given time k; $w_q(k)$ and $v_q(k)$ are white Gaussian noise with zero mean and covariances Q_q and R_q, respectively; and A_q, B_q, and C_q are the state space matrices corresponding to each flight mode. The measurement model in Eq. (2) can describe different levels of surveillance quality. For example, in Sec. IV, two different measurements models are considered: one assumes the radar measurements for current ATC scenarios, and one assumes the ADS-B data for future ATC scenarios.

The hybrid (or multiple model) system in Eqs. (1) and (2) has been used in various ATC applications [8–11]. In those papers, the flight mode transitions are assumed to be a Markov chain with constant probabilities of mode transitions that are independent of the continuous state. This assumption is not good for conformance monitoring applications. The task of conformance monitoring is to detect any deviations of an aircraft trajectory from its planned flight path, usually specified by a set of waypoints. Hence, it is necessary to model how the aircraft flight mode is expected to change in relation to, say, its position or distance (i.e., continuous state) from a given waypoint. Therefore, a more accurate model is needed to describe the aircraft mode transitions, which are dependent on flight plan and/or air route structure.

In this paper, we use an aircraft model proposed in our earlier work, which describes the flight mode transitions based on a set of stochastic guard conditions [12]. These guard conditions can be formulated, based on a given flight plan (or a set of waypoints) of the aircraft to describe the expected aircraft dynamics. The probabilities of flight mode transitions, which are dependent on the continuous state, can then be derived from the stochastic guard conditions.

It is modeled that a flight mode changes from $q(k-1) = i$ to $q(k) = j$ if a guard condition $G(i, j)$ is satisfied, where $G(i, j)$ is given by

$$G(i, j) = \{[x \quad \theta]^T | L_{x,ij}x + L_{\theta,ij}\theta \le 0\} \tag{3}$$

where $L_{x,ij} \in \mathbb{R}^{l\times n}$ and $L_{\theta,ij} \in \mathbb{R}^{l\times s}$ are constant matrices, and $\theta \in \mathbb{R}^s$ is a random vector with probability density function (PDF):

$$p[\theta] = \mathcal{N}_s(\theta;\, \bar{\theta},\, \Sigma_\theta) \tag{4}$$

We will see later that the random vector θ is used to describe the random deviations of the aircraft flight trajectories due to navigation uncertainties. The mean $\bar{\theta}$ can be determined based on the nominal flight path along the given flight plan or air route structure, and the covariance Σ_θ can be determined based on RNP or the navigation capabilities of the aircraft. Thus, the flight mode evolution is described by

$$q(k) = \gamma[q(k-1),\, x(k-1),\, \theta] \tag{5}$$

where γ: $\mathcal{Q} \times X \times \Theta \to \mathcal{Q}$ is the mode transition function defined as

$$\gamma(i,\, x,\, \theta) = j \tag{6}$$

if

$$[x^T \quad \theta^T]^T \in G(i, j)$$

Note that $Pr[\mathcal{A}]$ denotes the probability of an event $\mathcal{A}$. The continuous-state-dependent mode transition probability is then given by [13]:

$$\begin{aligned}\pi_{ij}(k-1)\text{: } & Pr[q(k) = j | q(k-1) = i,\, x] \\ &= Pr[L_{x,ij}x(k-1) + L_{\theta,ij}\theta \le 0 | x(k-1) = x] \\ &= \Phi_l(L_{\theta,ij}\bar{\theta} + L_{x,ij}x,\, L_{\theta,ij}\Sigma_\theta L_{\theta,ij}^T)\end{aligned} \tag{7}$$

where $\Phi_l(\mu,\, \Sigma)$ is the l-dimensional Gaussian cumulative density function (CDF), with a mean of μ and a covariance of Σ, defined as follows.

Definition: Suppose y is an l-dimensional Gaussian variable with a mean of μ and a covariance of Σ:

$$\Phi_l(\mu,\, \Sigma)\text{: } Pr[y \le 0]$$

Methods to compute the Gaussian CDF are discussed in our earlier paper [13] and the references therein.

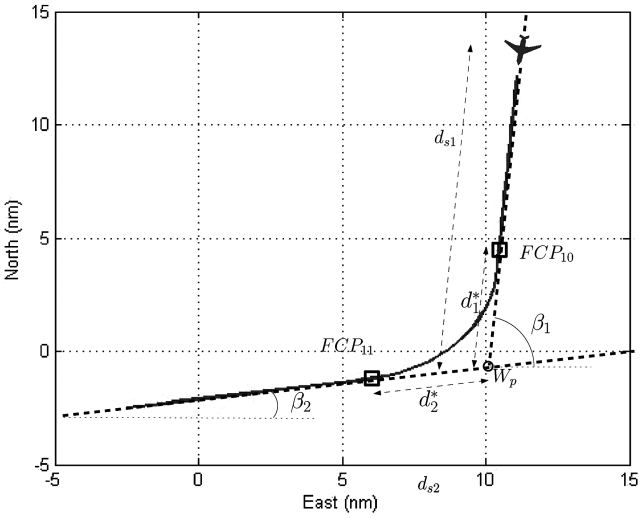

Fig. 2 An aircraft moving along a planned flight route.

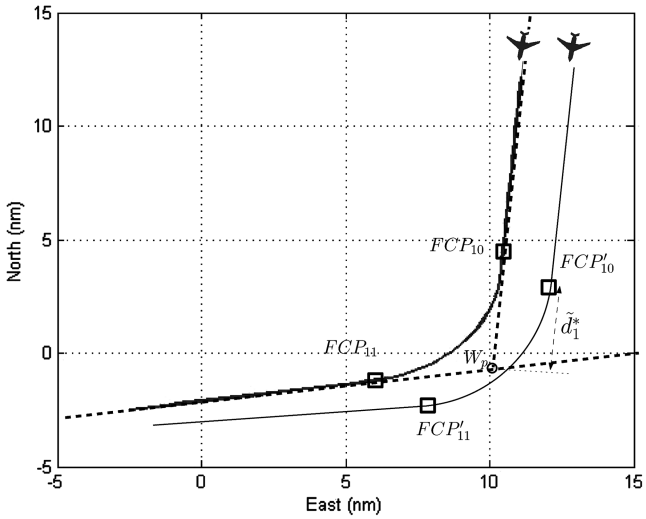

Fig. 3 A typical aircraft deviation from a standard flight route due to navigation uncertainties.

Example: The following example illustrates the flight mode transition model. It is assumed that an aircraft is following a standard flight route in a horizontal plane, as shown in Fig. 2. The flight route consists of two straight legs intersecting at a waypoint W_p. The aircraft dynamics are modeled as consisting of two flight modes: a CV mode and a CT mode. Along the standard flight route, the aircraft would start to turn (which corresponds to mode transition CV $\rightarrow$ CT) at the flight-trajectory change point FCP_{10} and complete the turn (which corresponds to mode transition CT $\rightarrow$ CV) at FCP_{11}. The points FCP_{10} and FCP_{11} are computed-based on a nominal turn radius (or turning rate of 1.5 deg/s). In practice, the points at which the aircraft starts to turn (or completes a turn) would deviate when the turn radius is different. We will discuss how this deviation is modeled in the latter part of this section. First, consider the mode transition when the aircraft is approaching FCP_{10}. The distance d_{s1} is defined to be the distance of the aircraft from W_p, projected along the direction of the first leg β_1. The distance is given by

$$d_{s1} = (\xi - \xi_{\text{ref}})\cos(\beta_1) + (\eta - \eta_{\text{ref}})\sin(\beta_1) \tag{8}$$

where $(\xi_{\text{ref}}, \eta_{\text{ref}})$ are the coordinates of W_p. Also, let d_1^* be the distance of FCP_{10} from W_p along the direction β_1. Then, the aircraft would start to turn when the guard condition $d_{s1} \le d_1^*$ is satisfied, or

$$\begin{bmatrix}\cos(\beta_1) & 0 & \sin(\beta_1) & 0 & 0 & 0\end{bmatrix} x - \theta_1 \le 0 \tag{9}$$

where $\theta_1 = d_1^* - \xi_{\text{ref}}\cos(\beta_1) - \eta_{\text{ref}}\sin(\beta_1)$.

In practice, the trajectory of a conforming aircraft could deviate from the nominal one due to navigation uncertainties, as illustrated in Fig. 3. To account for the uncertainties, the parameter d_1^* (or θ_1) in the guard condition is considered to be a random Gaussian variable. The mean of θ_1 is chosen, based on the nominal flight path, and its covariance is chosen to describe the expected deviations of typical aircraft trajectories, based on RNP or the aircraft navigation capabilities. This stochastic flight mode transition model differentiates the normal deviations for aircraft trajectories due to navigation uncertainties from those due to nonconforming actions, and hence helps to reduce the FARs and the mean detection delays.

Similarly, the distance d_{s2} is defined as the distance of the aircraft from W_p projected along the direction of the second leg β_2, and d_2^* is defined as the distance of FCP_{11} from W_p along the direction β_2. When the aircraft is approaching FCP_{11}, it is modeled that the flight mode switches from CT $\rightarrow$ CV when $d_{s2} \ge d_2^*$, or

$$\begin{bmatrix}-\cos(\beta_2) & 0 & -\sin(\beta_1) & 0 & 0 & 0\end{bmatrix} x + \theta_2 \le 0$$

where $\theta_2 = d_2^* - \xi_{\text{ref}}\cos(\beta_2) - \eta_{\text{ref}}\sin(\beta_2)$. Again, θ_2 is considered as a random variable to account for navigation uncertainties.

Thus, in general, the covariance Σ_θ in Eq. (4) describes the random deviations of typical flight profiles from the nominal, due to variations in aircraft turn radius, navigation uncertainties, etc. It could be determined, based on the RNP for current operations or based on the aircraft navigation performance for performance-based operations under the NEXTGEN. It has been shown in our earlier work that other aircraft flight trajectories, such as landing or takeoff profiles, can also be modeled using the mode transition model in Eqs. (3–6) [12].

III. Conformance Monitoring

As discussed in Sec. I, the conformance monitoring algorithm consists of a residual generation scheme and a decision making scheme. The residual generation scheme design is based on a hybrid estimation algorithm, known as the state-dependent transition hybrid estimation (SDTHE) algorithm, proposed in our earlier work [13]. The SDTHE algorithm is based on the well-known interacting multiple model (IMM) algorithm [14,15]. However, the IMM algorithm, which assumes constant mode transition probabilities, is not applicable to the SLHS in Eqs. (1–6), which has continuous-state-dependent mode transitions. The SDTHE algorithm is used to estimate the hybrid state (position, velocity, and flight mode) of the aircraft, based on the measurements, and then generate a residual. It will be shown that the generated residual has a zero mean and a known covariance if the aircraft is conforming to the flight plan. After obtaining the characteristics of this residual, a statistical decision making algorithm, called the Segen's algorithm, is implemented to test for conformance or nonconformance.

A. Residual Generation Filter

The residual generation filter is designed, based on the SDTHE algorithm. The SDTHE algorithm is a hybrid estimation algorithm, which estimates both the continuous state and the discrete state (or mode) for the SLHS in Eqs. (1–6).

The structure of the residual generation filter, based on the SDTHE algorithm, is shown in Fig. 4. The residual generation filter consists of a bank of n_d mode-matched Kalman filters, each matched to a mode of the hybrid system in Eqs. (1) and (2). Let Z^k denote the sequence of measurements $[z(1), z(2), \ldots, z(k)]$ and $p[\cdot|\cdot]$ denote a conditional PDF. Each Kalman filter j computes a continuous state estimate $\hat{x}_j(k)$ and its covariance $P_j(k)$, conditioned on the measurements Z^k and the event $q(k) = j$. The probability of flight mode $Pr[q(k)|Z^k]$ is also computed. Details of the algorithm are as follows.

First, the mode transition probabilities $\lambda_{ij}(k)$: $Pr[q(k) = j|q(k-1) = i, Z^{k-1}]$ are computed. It can be shown that the mode transition probability is given by [13]:

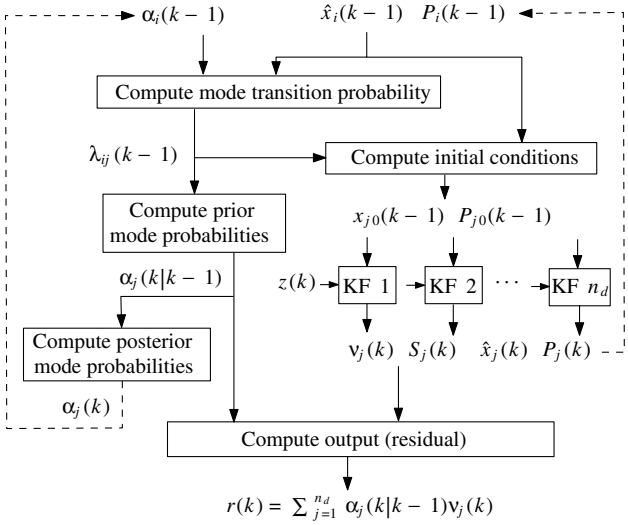

Fig. 4 Structure of the residual generation filter, based on the SDTHE algorithm (KF denotes Kalman filter).

$$\lambda_{ij}(k-1) = \int_{\mathbb{R}^n} \pi_{ij}(x)p[x(k-1)=x|q(k-1)=i, Z^{k-1}]\,\mathrm{d}x$$
$$= \Phi_l[L_{\theta,ij}\bar{\theta} + L_{x,ij}\hat{x}_i(k-1) + b_{ij},\ L_{\theta,ij}\Sigma_\theta L_{\theta,ij}^T + L_{x,ij}P_i(k-1)L_{x,ij}^T] \tag{10}$$

Note that the computational cost of evaluating $\lambda_{ij}(k-1)$ in Eq. (7) mainly depends on the dimension of the guards l, and it is independent of the dimensions n or m.

It is known that an exact Bayesian approach to update the continuous state estimates $\hat{x}_j(k)$ and the corresponding covariances $P_j(k)$ for a hybrid system requires an exponentially growing complexity, due to the exponentially growing number of mode histories [16]. A method proposed in the IMM algorithm is used to overcome this problem [14]. This method computes a mixed initial condition to each Kalman filter j as

$$\hat{x}_{j0}(k-1) = E[x(k-1)|q(k)=j, Z^{k-1}] = \sum_{i=1}^{n_d} \hat{x}_i(k-1)\gamma_{ji}(k-1) \tag{11}$$

$$P_{j0}(k-1) = E\{[x(k-1)-\hat{x}_{j0}(k-1)][x(k-1)-\hat{x}_{j0}(k-1)]^T|q(k)=j, Z^{k-1}]$$
$$= \sum_{i=1}^{n_d}\{P_i(k-1) + [\hat{x}_i(k-1)-\hat{x}_{j0}(k-1)][\hat{x}_i(k-1)-\hat{x}_{j0}(k-1)]^T\}\gamma_{ji}(k-1) \tag{12}$$

where

$$\gamma_{ji}(k-1): Pr[q(k-1)=i|q(k)=j, Z^{k-1}] = \frac{1}{c_j}\lambda_{ij}(k-1)Pr[q(k-1)=i|Z^{k-1}] \tag{13}$$

and c_j is a normalizing constant.

Each Kalman filter j then updates the continuous state estimates and computes the innovation $\nu_j(k)$ using the well-known equations:

$$\nu_j(k) = z(k) - C_jA_j\hat{x}_{j0}(k-1) \tag{14}$$

$$\hat{x}_j(k) = A_j\hat{x}_{j0}(k-1) + K_j(k)\nu_j(k) \tag{15}$$

$$P_j(k) = [I - K_j(k)C_j]P_j(k|k-1) \tag{16}$$

$$P_j(k|k-1) = A_jP_{j0}(k-1)A_j^T + Q_j \tag{17}$$

$$S_j(k) = C_jP_j(k|k-1)C_j^T + R_j \tag{18}$$

$$K_j(k) = P_j(k|k-1)C_j^TS_j^{-1}(k) \tag{19}$$

The probabilities of the flight modes are updated as follows:

$$\alpha_j(k): Pr[q(k)=j|Z^k] = \tfrac{1}{\delta}p[z(k)|q(k)=j, Z^{k-1}]Pr[q(k)=j|Z^{k-1}] \tag{20}$$

where δ is a normalizing constant, $p[z(k)|q(k)=j, Z^{k-1}]$ is the likelihood function given by

$$p[z(k)|q(k)=j, Z^{k-1}] = \mathcal{N}_p[\nu_j(k); 0, S_j(k)] \tag{21}$$

and $Pr[q(k)=j|Z^{k-1}]$ is the prior mode probability given by

$$\alpha_j(k|k-1): Pr[q(k)=j|Z^{k-1}] = \sum_{i=1}^{n_d}\lambda_{ij}(k-1)Pr[q(k-1)=i|Z^{k-1}] \tag{22}$$

The residual is defined as the difference between the measurement $z(k)$ and the expected measurement $\hat{z}(k)$, where

$$\hat{z}(k): E[z(k)|Z^{k-1}] = \sum_{j=1}^{n_d} E[C_{q(k)}x(k) + v_{q(k)}(k)|Z^{k-1}$$
$$q(k)=j]Pr[q(k)=j|Z^{k-1}] = \sum_{j=1}^{n_d}\alpha_j(k|k-1)C_jA_j\hat{x}_{j0}(k-1) \tag{23}$$

Thus, the output of the residual generation filter is the residual vector $r(k)$ given by

$$r(k): z(k) - \hat{z}(k) = z(k) - \sum_{j=1}^{n_d}\alpha_j(k|k-1)C_jA_j\hat{x}_{j0}(k)$$
$$= \sum_{j=1}^{n_d}\alpha_j(k|k-1)[z(k) - C_jA_j\hat{x}_{j0}(k-1)]$$
$$= \sum_{j=1}^{n_d}\alpha_j(k|k-1)\nu_j(k) \tag{24}$$

B. Characteristics of Residuals

To facilitate decision making for conformance monitoring, the statistical characteristics of the residual vector $r(k)$ need to be investigated. Let $r^s = [r(1), r(2), \ldots, r(s)]$ be a sequence of residuals up to time s. We consider only absolutely continuous probability distributions here. The complete probabilistic description of the sequence r^s can be given by a family of conditional PDFs $p[r(k)|r^{k-1}]$ for $k = 1, 2, \ldots, s$, where r^0 denotes the initial conditions for the residual generation filter at time $k = 0$. The conditional mean $\bar{r}(k)$: $E[r(k)|r^{k-1}]$ and covariance

$$\mathrm{cov}\,[r(k)|r^{k-1}]: E\{[r(k)-\bar{r}(k)][r(k)-\bar{r}(k)]^T|r^{k-1}\}$$

are first derived as follows.

The following fact is used in our derivations. From Eq. (24),

$$r(k) = z(k) - \sum_{j=1}^{n_d}\alpha_j(k|k-1)C_jA_j\hat{x}_{j0}(k-1) \tag{25}$$

From Eq. (25), given any initial conditions for the case $k = 0$, there is a 1–1 correspondence between the sequence of residuals r^k and the

sequence of measurements Z^k. Hence, $E[r(k)|r^{k-1}] = E[r(k)|Z^{k-1}]$, etc.

First, consider the innovation from each Kalman filter j at time k. Substituting Eqs. (1) and (2) into Eq. (14), we have

$$\nu_j(k) = C_{q(k)}A_{q(k)}x(k-1) - C_jA_j\hat{x}_{j0}(k-1) + C_{q(k)}w_{q(k)}(k) + v_{q(k)}(k) \tag{26}$$

At time k, the measurement sequence Z^{k-1} is known (or given). Therefore, the variable $\hat{x}_{j0}(k-1)$ is known. The unknown (or random) variables in Eq. (26) are the true state $x(k-1)$, the true mode $q(k)$, and the white zero-mean noise vectors $w_{q(k)}(k)$ and $v_{q(k)}(k)$. By taking the expectation conditioned on $q(k) = \varrho$ and the known measurement sequence Z^{k-1} on Eq. (26), we have

$$\begin{aligned} E[\nu_j(k)|q(k) = \varrho,\ Z^{k-1}] &= C_\varrho A_\varrho E[x(k-1)|q(k) \\ &= \varrho, Z^{k-1}] - C_jA_j\hat{x}_{j0}(k-1) = C_\varrho A_\varrho \hat{x}_{\varrho 0}(k-1) \\ &- C_jA_j\hat{x}_{j0}(k-1) \end{aligned} \tag{27}$$

Furthermore, by the theorem of total probability,

$$E[\nu_j(k)|Z^{k-1}] = \sum_{\varrho=1}^{n_d} E[\nu_j(k)|q(k) = \varrho, Z^{k-1}]\alpha_\varrho(k|k-1) \tag{28}$$

Hence, from Eqs. (24), (27), and (28), the mean of the conditional residual $r(k)$ is

$$\begin{aligned} E[r(k)|Z^{k-1}] &= \sum_{j=1}^{n_d} \alpha_j(k|k-1)E[\nu_j(k)|Z^{k-1}] \\ &= \sum_{j=1}^{n_d}\sum_{\varrho=1}^{n_d} \alpha_j(k|k-1)\alpha_\varrho(k|k-1)[C_\varrho A_\varrho \hat{x}_{\varrho 0}(k-1) \\ &- C_jA_j\hat{x}_{j0}(k-1)] = 0 \end{aligned} \tag{29}$$

Next, the covariance terms are computed. We consider the covariance of the Kalman filter innovations conditioned on $q(k) = \varrho$. Let $\bar{\nu}_j(k|\varrho) = E[\nu_j(k)|q(k) = \varrho, Z^{k-1}]$. Using Eqs. (18), (26), and (27), the cross covariance of the innovations $\nu_i(k)$ and $\nu_j(k)$ are derived as

$$\begin{aligned} \mathrm{Cov}[\nu_i(k), \nu_j(k)|q(k) = \varrho, Z^{k-1}]&: E[[\nu_i(k) - \bar{\nu}_i(k|\varrho)] \\ \times [\nu_j(k) - \bar{\nu}_j(k|\varrho)]^T|q(k) &= \varrho,\ Z^{k-1}] \\ = C_\varrho A_\varrho \mathrm{cov}[(x(k-1)|q(k) &= \varrho,\ Z^{k-1}]A_\varrho^T C_\varrho^T + C_\varrho Q_\varrho C_\varrho^T + R_\varrho \\ = C_\varrho A_q P_{\varrho 0}(k-1)A_\varrho^T C_\varrho^T &+ C_\varrho Q_\varrho C_\varrho^T + R_\varrho = S_\varrho(k) \end{aligned} \tag{30}$$

Hence,

$$\begin{aligned} \mathrm{Cov}[\nu_i(k),\ \nu_j(k)|Z^{k-1}] &= \sum_{\varrho=1}^{n_d} \mathrm{Cov}[\nu_i(k),\ \nu_j(k)|q(k) \\ = \varrho, Z^{k-1}]Pr[q(k) = \varrho|Z^{k-1}] &= \sum_{\varrho=1}^{n_d} \alpha_\varrho(k|k-1)S_\varrho(k) \end{aligned} \tag{31}$$

From Eqs. (24) and (31), the covariance of residual $r(k)$ is

$$\begin{aligned} \Sigma(k)&: \mathrm{Cov}[r(k)|Z^{k-1}] \\ &= \sum_{i=1}^{n_d}\sum_{j=1}^{n_d} \alpha_i(k|k-1)\alpha_j(k|k-1)\mathrm{Cov}[\nu_i(k),\ \nu_j(k)|Z^{k-1}] \\ &= \sum_{\varrho=1}^{n_d} \alpha_\varrho(k|k-1)S_\varrho(k) \end{aligned} \tag{32}$$

In the residual generation filter, it is assumed that the conditional PDF $p[\nu_j(k)|Z^{k-1}]$ is Gaussian. This is a common assumption in multiple model algorithms, including the IMM algorithm [9]. From Eq. (24), under the Gaussian approximation, the conditional PDF $p[r(k)|r^{k-1}]$ is also Gaussian. Thus, from the previous results, under the hypothesis that the aircraft is conforming to the trajectory modeled by the SLHS,

$$p[r(k)|r^{k-1}] \approx \mathcal{N}_p[r(k);\ 0,\ \Sigma(k)] \tag{33}$$

C. Decision Making

A nonconformance is defined as a deviation of the aircraft behavior from the nominal one modeled by the SLHS. Using the result in Sec. III.B, if a nonconformance occurs at time k_0, then (assuming Eq. (33) to be exact)

$$p[r(k)|r^{k-1}] = \mathcal{N}_p[r(k);\ 0,\ \Sigma(k)]$$

almost surely for

$$k = 0,\ 1,\ \ldots,\ k_0 - 1$$

and

$$Pr\{p[r(k)|r^{k-1}] \neq \mathcal{N}_p[r(k); 0, \Sigma(k)]\} > 0$$

for

$$k \geq k_0$$

At each time k_c, where $k_c = 1, 2, \ldots$, we wish to determine if a nonconformance has occurred. The nonconformance detection problem can be formulated as a test of the hypotheses:

$$\begin{aligned} H_0&: k_0 > k_c \quad \text{(conformance)} \\ H_1&: k_0 \leq k_c \quad \text{(non-conformance)} \end{aligned}$$

The following test, based on the work of Segen and Sanderson [17], is constructed. Let

$$\beta(k) = \int p[r|r^{k-1}]\log(p[r|r^{k-1}])\ \mathrm{d}r - \log(p[r|r^{k-1}])$$

$$\zeta(k) = \frac{1}{\sigma_\beta}\sum_{i=1}^{k} \beta(i)$$

where σ_β^2 is the variance of the sequence of $\beta(i)$.

Under the null hypothesis H_0,

$$\beta(k) = \tfrac{1}{2}[r^T(k)\Sigma^{-1}(k)r(k) - p]$$

$$\zeta(k) = \frac{1}{\sqrt{2p}}\sum_{i=1}^{k}[r^T(i)\Sigma^{-1}(i)r(i) - p]$$

where p is the dimension of the measurement vector. The test statistic is defined as

$$\tau(k) = \frac{1}{\sqrt{k}}\max_{1\leq i\leq k}\zeta(i)$$

The null hypothesis is rejected if

$$\tau(k) > \tau_\alpha \tag{34}$$

where τ_α is a constant that determines the significance level (or probability of rejecting H_0 when H_0 is true) of the test. The significance level of the test can be approximated using the limiting distribution of $\tau(k)$ [17]:

$$\lim_{k\to\infty} Pr[\tau(k) \leq \tau_\alpha] = \sqrt{\frac{2}{\pi}}\int_0^{\tau_\alpha} e^{-t^2/2}\ \mathrm{d}t$$

A large τ_α yields a small significance level, and hence a small probability of false alarms, at the expense of higher detection delays. However, an exact relation between the significance level and the

probability of false alarms has yet to be established, and this could be a topic in future research.

IV. Simulation Examples

A. Aircraft Dynamics and Measurement Models

In this section, the conformance monitoring algorithm is illustrated with two examples: 1) a waypoint transition in a horizontal plane; and 2) an altitude transition in a vertical plane. The SLHS is used to model the dynamics of the conforming aircraft in the respective scenarios. In the horizontal plane, the SLHS consists of two modes: a CV mode and a CT mode. In the CV mode, the aircraft flies at a CV, and in the CT mode, the aircraft turns at a constant turning rate. In the vertical plane, the SLHS consists of a constant height (CH) mode and a constant descent (CD) mode. In the CH mode, the aircraft flies at a constant altitude (CA), and in the CD mode, the aircraft descends with a CA rate. The dynamic models of the various flight modes used in this paper are given in the Appendix. The proposed algorithm does not impose any restriction on the complexity of the dynamic models of the flight modes. Hence, more complex models may be used to describe more complex trajectories, such as a turn with changing turning rates, in future research.

We consider two cases with different measurement models. In the first case, which corresponds to a typical current ATC scenario, it is assumed that aircraft horizontal positions are measured by a surveillance radar with an update interval of $T_s = 6$ s, and the aircraft altitudes are reported by a mode C transponder. Typically, radar measurements are reported in polar coordinates, and accuracy depends on the range. It is assumed that the measurements are transformed into Cartesian coordinates (as latitudes/longitudes). Furthermore, because the simulations are of short durations, it is assumed that the position errors have a constant standard deviation of 300 ft in each axis of the Cartesian coordinates [9]. The mode C altitude information is coded and has a discrete error of $\sigma_h = 100$ ft. In our measurement model, the altitude measurement noise is approximated as a Gaussian noise, with variance $\frac{1}{12}\sigma_h^2$. In the second case, an ATC scenario in the NEXTGEN, in which aircraft positions (latitudes, longitudes, and altitudes) are reported by the onboard ADS-B system, is considered. The standard deviations of the latitude and longitude position errors are both 65 ft, and the standard deviation of the altitude error is 30 ft. The data update interval is $T_s = 1$ s [18].

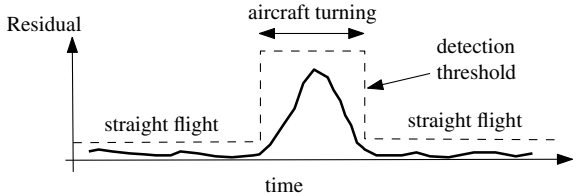

Fig. 5 Typical plot of a residual generated without modeling trajectory deviations, due to uncertainties during turns [1].

B. Waypoint Transition in the Horizontal Plane

We consider the conformance monitoring of an aircraft moving along a flight route with a waypoint transition, as illustrated in Fig. 2. Conformance monitoring for a similar flight scenario has been considered by Reynolds and Hansman [1]. In their paper, the authors use a CR, which is generated by a difference between the observed and expected state values (e.g., position and/or heading) for conformance monitoring. The expected state values are computed, based on an aircraft dynamic model, which assumes that the aircraft trajectory follows the planned flight route exactly. However, as illustrated in Fig. 3, a typical aircraft trajectory could deviate significantly from the assumed trajectory, due to factors such as navigation uncertainties, winds, and unknown pilot intents (e.g., commanded turn radius). The result of this is that the CR generated will have a significant error during the turn (or waypoint transition) [1]. A typical plot of such residuals for an aircraft conforming to the flight plan is shown in Fig. 5. Thus, a detection threshold of approximately 10 times higher is required during turns than during straight flights. This higher detection threshold during turns significantly increases the mean detection delay for a given FAR.

In our proposed conformance monitoring scheme, the SDTHE algorithm generates the residual, based on the SLHS, which (as described in Sec. II) models the expected deviations of aircraft trajectories near a waypoint. Thus, the residual generated has approximately a zero mean during both straight flights and turns. A plot of a typical residual from the SDTHE algorithm is shown in Fig. 6.

The performance of the conformance monitoring algorithm is evaluated, based on FARs and mean detection delays. Clearly, a small mean detection delay for a given FAR is desired. To compute the FARs, a set of random aircraft trajectories are first generated around the planned flight path (see Fig. 7). These trajectories are assumed to be conforming to the flight plan, but they deviate randomly, with a standard deviation of 1 nm in each axis from the planned flight path, due to navigation uncertainties. Note that Fig. 7

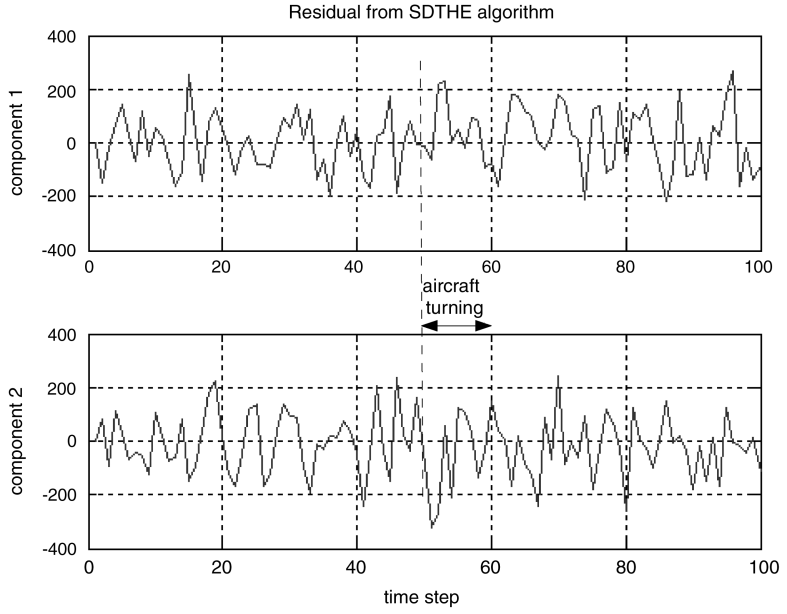

Fig. 6 Typical plot of a residual generated by the SDTHE algorithm, which accounts for trajectory deviations. The residual for a conforming aircraft does not significantly deviate from a zero mean during a turn.

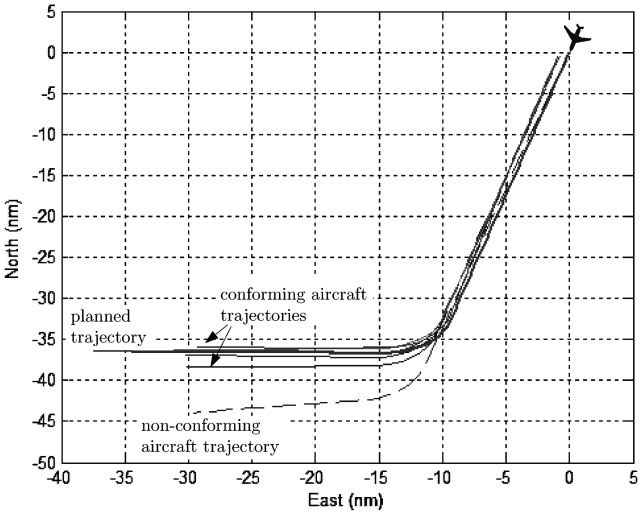

Fig. 7 Plots of some simulated trajectories in the horizontal plane.

shows just some of the simulated aircraft trajectories. The conformance monitoring algorithm is then used to detect any nonconformance, based on measurements from radar and ADS-B, respectively. The FAR is computed as

$$\text{FAR} = \frac{N_d}{N_{\text{con}}}$$

where N_d is the number of nonconformance detected by the conformance monitoring algorithm and N_{con} is the number of simulated conforming trajectories. We use $N_{\text{con}} = 2000$ in this example.

Next, the mean detection delay of the conformance monitoring algorithm is computed. A set of nonconforming trajectories, similar to the one shown in Fig. 7, is generated. Because we are interested in the mean detection delays during the mode transition or turning phase (which has much higher delays than during straight flights), the simulated nonconforming trajectories all start to deviate from the planned flight path during or at the end of the turn. Let $t_d^{(i)}$ be the time when a nonconformance is detected and $t_{\text{nc}}^{(i)}$ be the time when the aircraft is supposed to start the CT along the planned trajectory for an ith simulation run. The mean detection delay is computed as

$$\bar{T}_d = \sum_{i=1}^{N_{\text{nc}}} \frac{(t_d^{(i)} - t_{\text{nc}}^{(i)})}{N_{\text{nc}}}$$

where N_{nc} is the number of nonconforming trajectories simulated.

In the proposed algorithm, the mode transition is modeled using the stochastic guards described in the example in Sec. II. The parameters θ_1 and θ_2 are assumed to be random parameters, each with a standard deviation of 1 nm to account for the random trajectory deviations. In practice, the standard deviations of the parameters could vary, depending on the RNP or navigation accuracy of the aircraft. The tradeoff between FAR and mean detection delays is determined by the detection threshold τ_α in Eq. (34). Plots of the FAR versus the mean detection delays are given in Fig. 8. The results of the proposed algorithm are compared with the results in Reynolds and Hansman's paper [1] (or the CR algorithm). For the CR algorithm, only a simulation result with ADS-B data is available. Because of the lack of sufficient information, our simulation scenario is not exactly the same as the scenario considered by Reynolds and Hansman. However, we have done our best to match them. For example, our measurement model using the ADS-B data is the same as that in Reynolds and Hansman's paper. Thus, we believe that the results in Fig. 8 illustrate that our proposed algorithm could yield significantly better performance than the CR algorithm. For example, with FAR = 0.2, our algorithm yields approximately 6 and 12 s mean detection delays, using ADS-B data and radar data, respectively, whereas the CR algorithm yields approximately a 105 s mean detection delay using ADS-B data. This improved performance is a

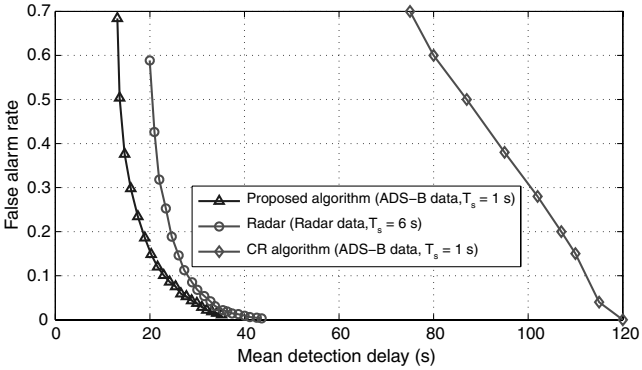

Fig. 8 Plots of FARs versus mean detection delays for horizontal conformance monitoring.

result of the better aircraft model, as well as the more effective residual generation and decision making scheme, used in our proposed algorithm.

An essential idea in our proposed algorithm is in the use of stochastic guards to model the flight mode transitions, which results in the continuous-state-dependent mode transition probabilities given in Eq. (7). To illustrate the implications of this idea, we consider an alternative flight mode transition model that uses constant mode transition probabilities. This alternative model is based on the idea of the variable structure IMM (VSIMM) algorithm [19]. The VSIMM algorithm is an extension of the IMM algorithm, in which the mode set is variable (selected out of a finite number of mode sets). However, the mode transition probabilities within each mode set are constant. Here, we consider an alternative model for the flight mode transitions, based on the VSIMM algorithm as follows. We consider a VSIMM algorithm that consists of two mode sets. Each mode set consists of a CV mode (mode 1) and a CT mode (mode 2), as in the SLHS model. Let π_{ij} denote the probability of a mode transition from mode i to mode j. When the guard in Eq. (11) is satisfied, we use the mode set, with mode transition probabilities given by

$$\Pi = \begin{bmatrix} \pi_{11} & \pi_{12} \\ \pi_{21} & \pi_{22} \end{bmatrix} = \begin{bmatrix} 1 - p_{\text{CT}} & p_{\text{CT}} \\ 1 - p_{\text{CT}} & 1 - p_{\text{CT}} \end{bmatrix}$$

where p_{CT} is a constant that describes the probability of a CT flight mode. Otherwise, we use the mode set with mode transition probabilities given by

$$\Pi = \begin{bmatrix} \pi_{11} & \pi_{12} \\ \pi_{21} & \pi_{22} \end{bmatrix} = \begin{bmatrix} p_{\text{CV}} & 1 - p_{\text{CV}} \\ p_{\text{CV}} & 1 - p_{\text{CV}} \end{bmatrix}$$

where p_{CV} is a constant that describes the probability of a CV flight mode. Many different designs of the VSIMM algorithm are possible. Here, three designs of the VSIMM algorithm are considered for the purpose of comparison: 1) VSIMM1: $p_{\text{CV}} = p_{\text{CT}} = 0.8$; 2) VSIMM2: $p_{\text{CV}} = p_{\text{CT}} = 0.9$; and 3) VSIMM3: $p_{\text{CV}} = p_{\text{CT}} = 0.99$.

The performance of our proposed algorithm is compared against those of conformance monitoring, based on the previous VSIMM models. In the proposed algorithm, the mode transition probabilities are given by Eq. (7), whereas in the VSIMM-based algorithm, the mode transition probabilities are given as described previously. Plots of the mode transition probabilities π_{11} of the various algorithms are given in Fig. 9. In the limit $p_{\text{CV}} = p_{\text{CT}} \to 1$, the VSIMM algorithm would have the same mode transition model as that of a hybrid system with deterministic guards. A stochastic hybrid system model, based on deterministic guards, has been proposed by Hu et al. [20]. From Fig. 10, the proposed algorithm performs significantly better than the various VSIMM designs, especially for small FARs. Also, the performances of the VSIMM-based methods are sensitive to the choice of the mode transition probabilities. The case $p_{\text{CV}} = p_{\text{CT}} = 0.9$ yields the best performance among the three VSIMM designs. Although it may be possible to achieve better performance with other

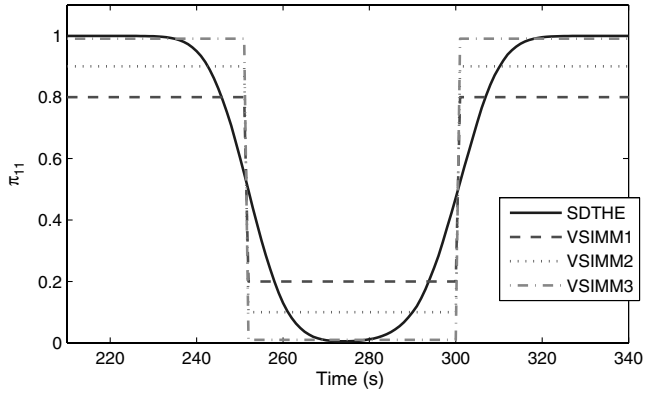

Fig. 9 Plots of mode transition probabilities π_{11} of the various algorithms.

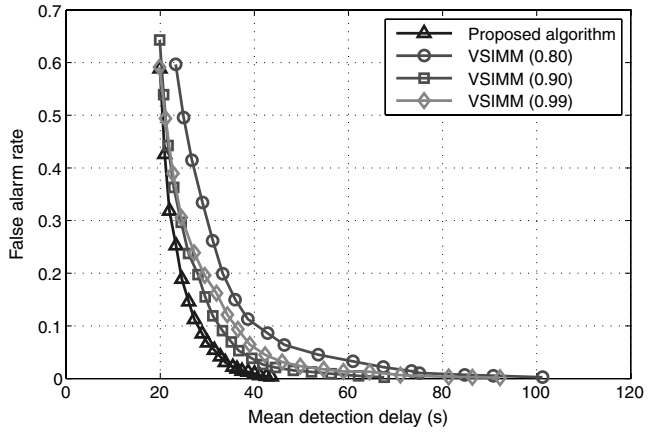

Fig. 10 Comparison of proposed algorithm versus conformance monitoring, based on the VSIMM algorithm. The results are for horizontal conformance monitoring with radar data.

designs of the VSIMM-based method, this would be a time consuming task. On the other hand, we can achieve good performance with the SDTHE algorithm, in which the SLHS model can be easily determined, based on the nominal aircraft trajectory and the expected navigation uncertainties.

C. Altitude Transition in the Vertical Plane

The performance of the conformance monitoring algorithm during altitude transitions in the vertical plane is illustrated in this section. Conformance monitoring in the vertical plane is a challenging task, due to both the presence of navigation uncertainties and the large number of vertical automation modes [1]. We use a vertical transition scenario, which is similar to the one used in Reynolds and Hansman, to demonstrate some of the challenges. The simulated aircraft trajectories are shown in Fig. 11. In this figure, there are three possible types of conforming aircraft trajectories: 1) altitude transitions from 30,000 ft to 25,000 ft under vertical speed (V/S) autopilot mode with a CD rate of 1500 ft/ min; 2) similar altitude transitions under flight-level change (FLCH) autopilot mode, with the descent profile calculated by the flight management system; and 3) similar altitude transitions under the FLCH autopilot mode with speedbrakes deployed. Note that each of these types of trajectories represents a realistic descent profile of a conforming aircraft. The typical trajectory of a nonconforming aircraft that is simulated in order to investigate the detection delays of the proposed algorithm is plotted in Fig. 11.

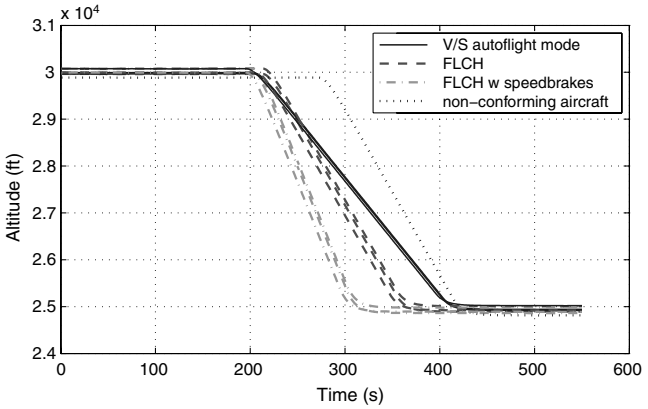

Fig. 11 Some simulated aircraft trajectories in the vertical plane.

Because a conforming aircraft may follow one of the three types of trajectories described previously, it is difficult to carry out conformance monitoring with a single SLHS model. To overcome this problem, a conformance monitoring scheme, illustrated in Fig. 12, is used. It consists of three SLHS models, each of which describes one type of conforming descent trajectory. Conformance monitoring is then carried out by parallel hypothesis tests, based on the respective SLHS models. For example, the SLHS1 model describes the trajectories of the V/S autopilot descent. We use the proposed decision making algorithm to test if an aircraft is descending with the V/S autopilot mode; that is, we test the hypotheses:

$$H_0\text{: V/S autopilot mode} \quad H_1\text{: not V/S autopilot mode}$$

Next, based on the result of the statistical test, we define a decision variable D_{c1} as

$$D_{c1} = \begin{cases} 0 & \text{if } H_0 \text{ is true} \\ 1 & \text{if } H_1 \text{ is true} \end{cases}$$

Similarly, hypothesis tests based on the SLHS2 and SLHS3 models are carried out to obtain the decision variables D_{c2} and D_{c3}. The conformance decision variable D_c is defined as

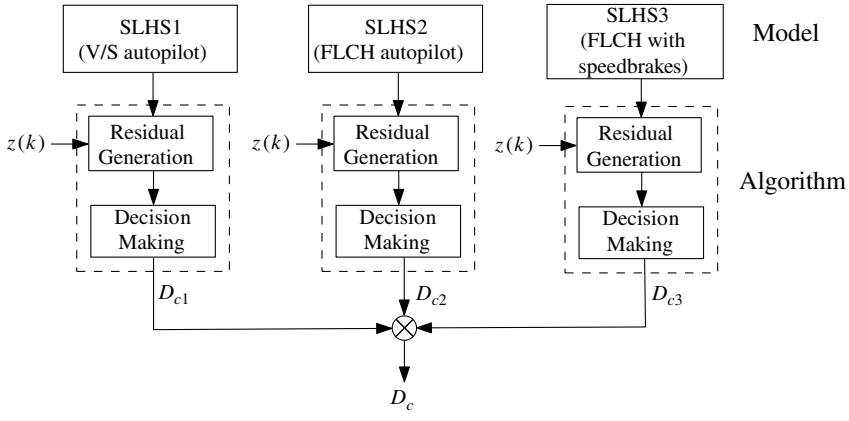

Fig. 12 Structure of the proposed vertical conforming monitoring scheme.

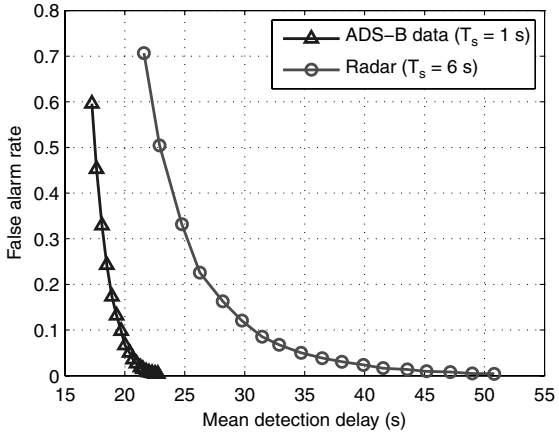

Fig. 13 Plots of FARs versus mean detection delays from the proposed algorithm for vertical conformance monitoring.

$$D_c = D_{c1} \times D_{c2} \times D_{c3}$$

A nonconformance is declared if $D_c = 1$. It is obvious that this is the case if, and only if, $D_{c1} = D_{c2} = D_{c3} = 1$; that is, the respective alternative hypotheses H_1 is true in all three tests.

The performance of the conformance monitoring scheme in this example is shown in Fig. 13. The results suggest that the proposed conformance monitoring scheme could be effective for complex ATC operating scenarios, such as the one illustrated in this example. Although the previously mentioned altitude transition scenario was first described by Reynolds and Hansman, they have not presented any corresponding conformance monitoring schemes nor results for this scenario. Thus, our proposed scheme is the first attempt to solve the conformance monitoring problem in this kind of complex ATC scenario. The results in Fig. 13 show good performance from the proposed algorithm. For example, with FAR $= 0.1$, the mean detection delay with ADS-B data is about 5 s (or five sampling intervals) and, with radar data, it is about 16 s (or less than three sampling intervals).

This example is used to illustrate the feasibility of using multiple hypothesis testing for conformance monitoring of vertical flight profiles involving more than one possible flight mode. In practice, vertical conformance monitoring is very hard, due to many factors, such as wind or aircraft mass, which may affect the possible vertical flight modes and trajectories. In the current example, the starting point of the altitude transition may also be uncertain, due to unknown pilot intents. One way to model this uncertainty is to use different SLHS models, as in Fig. 12, to describe the various possible starting points of the descent. Thus, more work needs to be done to improve the modeling of aircraft trajectories that take into consideration the many variations of the possible flight profiles.

V. Conclusions

An algorithm for conformance monitoring in ATC, based on SLHS modeling and fault detection techniques, has been proposed. The algorithm first generates a residual, which is expected to have a zero and a known covariance if the observed aircraft trajectory conforms to its flight plan or clearance. A statistical decision making algorithm is then implemented, based on a statistical test of the residual. It has been validated that the proposed conformance monitoring algorithm yields good performance in challenging ATC scenarios.

The results in our simulation examples illustrate that the proposed algorithm could handle various kinds of operational scenarios, including NEXTGEN scenarios (as well as various types of aircraft) in ATC conformance monitoring. However, due to the many possible variations in aircraft flight profiles in practice, further work needs to be done to investigate its effectiveness in actual applications. In future work, we would like to investigate the performance of the proposed algorithm with other ATC operational scenarios.

Appendix

Let (ξ, η, h) denote the position of the aircraft in Cartesian coordinates, for which h is the aircraft altitude. In the horizontal plane, the aircraft dynamics consist of a CV flight mode and a CT flight mode, which are described as follows:

CV mode:

$$\begin{bmatrix} \xi(k) \\ \dot{\xi}(k) \\ \eta(k) \\ \dot{\eta}(k) \end{bmatrix} = \begin{bmatrix} 1 & T_s & 0 & 0 \\ 0 & 1 & 0 & 0 \\ 0 & 0 & 1 & T_s \\ 0 & 0 & 0 & 1 \end{bmatrix} \begin{bmatrix} \xi(k-1) \\ \dot{\xi}(k-1) \\ \eta(k-1) \\ \dot{\eta}(k-1) \end{bmatrix} + \begin{bmatrix} \frac{T_s^2}{2} & 0 \\ T_s & 0 \\ 0 & \frac{T_s^2}{2} \\ 0 & T_s \end{bmatrix} \begin{bmatrix} w_{\xi_1}(k) \\ w_{\eta_1}(k) \end{bmatrix} \tag{35}$$

where T_s is the sampling period (we assume $T_s = 6$ s for radar data and $T_s = 1$ s for ADS-B data), and $w_{\xi_1}(k)$ and $w_{\eta_1}(k)$ are the white Gaussian noise with zero mean and covariance Q_{CV}.

CT mode:

$$\begin{bmatrix} \xi(k) \\ \dot{\xi}(k) \\ \eta(k) \\ \dot{\eta}(k) \end{bmatrix} = \begin{bmatrix} 1 & T_s & 0 & \frac{-\dot{\psi}T_s^2}{2} \\ 0 & 1 & 0 & -\dot{\psi}T_s \\ 0 & \frac{\dot{\psi}T_s^2}{2} & 1 & T_s \\ 0 & \dot{\psi}T_s & 0 & 1 \end{bmatrix} \begin{bmatrix} \xi(k-1) \\ \dot{\xi}(k-1) \\ \eta(k-1) \\ \dot{\eta}(k-1) \end{bmatrix} + \begin{bmatrix} \frac{T_s^2}{2} & 0 \\ T_s & 0 \\ 0 & \frac{T_s^2}{2} \\ 0 & T_s \end{bmatrix} \begin{bmatrix} w_{\xi_2}(k) \\ w_{\eta_2}(k) \end{bmatrix} \tag{36}$$

where $\dot{\psi}$ represents a nominal turning rate, and w_{ξ_2} and w_{η_2} are the white Gaussian noise with zero mean and covariance Q_{CT}. In our example in Sec. IV, we use a nominal turning rate of $\dot{\psi} = 1.5$ deg/s. The white noise w_{ξ_2} and w_{η_2} account for deviations of the actual turning rate from the nominal.

In the vertical plane, the flight modes are the CA mode:

$$h(k) = h(k-1) + T_s w_{h1}(k)$$

and the CD mode:

$$h(k) = h(k-1) + T_s \dot{h}_d + T_s w_{h2}(k)$$

where $\dot{h}_d$ is the descent rate, and $w_{h1}(k)$ and $w_{h2}(k)$ are the white Gaussian noise variables. In the altitude transition scenario in Sec. IV,

$$\dot{h}_d = \begin{cases} -1500 \text{ ft/min} & \text{during V/S autopilot mode} \\ -2100 \text{ ft/min} & \text{during FLCH autopilot mode} \\ -3000 \text{ ft/min} & \text{during FLCH with speed brakes} \end{cases}$$

Acknowledgments

The authors would like to acknowledge that this work is supported by the National Science Foundation CAREER award CNS-0746299 and to thank Helen Gill for her support.

References

[1] Reynolds, T. G., and Hansman, J. R., "Investigating Conformance Monitoring Issues in Air Traffic Control Using Fault Detection Techniques," *Journal of Aircraft*, Vol. 42, No. 5, Sept.–Oct. 2005, pp. 1307–1317.
doi:10.2514/1.10055

[2] Krishnamurthy, K., Barmore, B., Bussink, F., Weitz, L., and Dahlene, L., "Fast-Time Evaluations of Airborne Merging and Spacing in Terminal Arrival Operations," AIAA Guidance, Navigation, and Control Conference, AIAA Paper 2005-6143, Aug. 2005.

[3] Anon., "Concept of Operations for the Next Generation Air Transportation System," TR, Joint Planning and Development Office, Washington, D.C., Feb. 2007.

[4] "RTCA Task Force 3 Final Report on Free Flight Implementation," TR, RTCA, Inc., Washington, D.C., 1995.

[5] Gibbs, W. W., "Free-for-All Flights," *Scientific American*, Vol. 273, No. 6, Dec. 1995, pp. 34–37.

[6] Reynolds, T. G., and Hansman, R. J., "Conformance Monitoring Approaches in Current and Future Air Traffic Control Environments," *Proceedings of the 21st Digital Avionics Systems Conference*, Vol. 2, IEEE Publications, Piscataway, NJ, Oct. 2002, pp. 1–12. doi:10.1109/DASC.2002.1052922

[7] Brinton, C. R., and Atkins, S. C., "Analysis of Taxi Conformance Monitoring Algorithms and Performance," *Integrated Communications, Navigation, and Surveillance Conference*, IEEE Publications, Piscataway, NJ, April–May 2007, pp. 1–8. doi:10.1109/ICNSURV.2007.384165

[8] Li, X. R., and Bar-Shalom, Y., "Design of an Interacting Multiple Model Algorithm for Air Traffic Control Tracking," *IEEE Transactions on Control Systems Technology*, Vol. 1, No. 3, 1993, pp. 186–194. doi:10.1109/87.251886

[9] Bar-Shalom, Y., Rong Li, X., and Kirubarajan, T., *Estimation with Applications to Tracking and Navigation*, Wiley, New York, 2001, pp. 441–475.

[10] Hwang, I., Balakrishnan, H., and Tomlin, C., "State Estimation for Hybrid Systems: Applications to Aircraft Tracking," *IEE Proceedings of Control Theory and Applications*, Vol. 153, No. 5, 2006, pp. 556–566. doi:10.1049/ip-cta:20050053

[11] Hwang, J., Hwang, I., and Tomlin, C., "Flight-Mode-Based Aircraft Conflict Detection Using a Residual-Mean Interacting Multiple Model Algorithm," AIAA Guidance, Navigation and Control Conference, AIAA Paper 2003-5340, Aug. 2003.

[12] Hwang, I., and Seah, C. E., "A Hybrid Estimation Algorithm for Terminal-Area Aircraft Tracking," AIAA Guidance, Navigation, and Control Conference and Exhibit, AIAA Paper 2007-6691, Aug. 2007.

[13] Seah, C. E., and Hwang, I., "Stochastic Linear Hybrid Systems: Modeling, Estimation, and Application in Air Traffic Control," *IEEE Transactions on Control Systems Technology*, 2009 (accepted for publication).

[14] Blom, H. A. P., and Bar-Shalom, Y., "The Interacting Multiple Model Algorithm for Systems with Markovian Switching Coefficients," *IEEE Transactions on Automatic Control*, Vol. 33, No. 8, 1988, pp. 780–783. doi:10.1109/9.1299

[15] Seah, C. E., and Hwang, I., "State Estimation for Stochastic Linear Hybrid Systems with Continuous-State-Dependent Transitions: An IMM Approach," *IEEE Transactions on Aerospace and Electronic Systems*, Vol. 45, No. 1, 2009, pp. 376–392. doi:10.1109/TAES.2009.4805286

[16] Ackerson, G. A., and Fu, K. S., "On State Estimation in Switching Environments," *IEEE Transactions on Automatic Control*, Vol. 15, No. 1, 1970, pp. 10–17. doi:10.1109/TAC.1970.1099359

[17] Segen, J., and Sanderson, A. C., "Detecting Change in a Time Series," *IEEE Transactions on Information Theory*, Vol. 26, No. 2, March 1980, pp. 249–255. doi:10.1109/TIT.1980.1056151

[18] RTCA Special Committee SC-186, "Minimum Aviation System Performance Standards for the Automatic Surveillance-Broadcast (ADS-B)," Rept. DO-242A, RTCA, Inc., Washington, DC, Jan. 1998.

[19] Ru, J., and Rong Li, X., "Variable-Structure Multiple-Model Approach to Fault Detection, Identification, and Estimation," *IEEE Transactions on Control Systems Technology*, Vol. 16, No. 5, 2008, pp. 1029–1038. doi:10.1109/TCST.2007.916318

[20] Hu, J., Lygeros, J., and Sastry, S., "Towards a Theory of Stochastic Hybrid Systems," *Hybrid Systems: Computation and Control*, Vol 1790, Lecture Notes in Computer Science, Springer–Verlag, New York, 2000, pp. 160–173.